Appl. Phys. B 70, 231–235 (2000) / Digital Object Identifier (DOI) 10.1007/s003409900119

Applied Physics B
Lasers
and Optics
© Springer-Verlag 2000

On the performance of an ArF and a KrF laser as a function of the preionisation timing and the excitation mode

L. Feenstra, O.B. Hoekstra, P.J.M. Peters, W.J. Witteman

University of Twente, P.O. Box 217, 7500 AE Enschede, The Netherlands
(Fax: +31-53/489-1102, E-mail: L.Feenstra@tn.utwente.nl)

Received: 23 February 1999/Revised version: 4 June 1999/Published online: 16 September 1999

Abstract. An X-ray preionised ArF and KrF excimer laser has been studied with three different spiker-sustainer excitation circuits. We observed large differences in the laser performance, when the preionisation delay timing was varied on a nanosecond timescale. The behaviour of both lasers was found to be equivalent. The observations can be understood by considering the effect of the discharge excitation technique on the preionisation process. An excitation mode with a prepulse well above the steady-state voltage V_{SS} with a subsequent reversed overshoot voltage for initiating the discharge, in combination with a well-timed preionisation pulse is found to give the best results. Optimum output energies of 50 mJ with ArF and 175 mJ with KrF were obtained from an active volume of $60 \times 1.5 \times 1.2$ cm in the so-called swing mode, with the preionisation applied 60 ns before the discharge breakdown.

PACS: 42.55.Lt; 42.60.By; 52.80.Tn

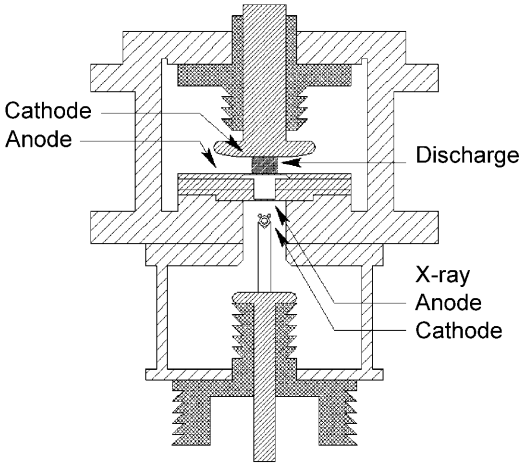

Fig. 1. The laser vessel and the X-ray source. The discharge volume is preionised through the laser anode. The X-ray source and the laser gas mixture are separated by the 1-mm-thick aluminium pressure window annex X-ray anode

The goal of our research is the construction of long-pulse, high-output-power, discharge-pumped ArF ($\lambda = 193$ nm) and KrF ($\lambda = 248$ nm) excimer lasers with a high beam quality. In accordance with previous successful developments on excimer lasers, the starting point is X-ray preionisation and spiker-sustainer excitation [1, 2], whereas for the buffer gas He was chosen [3–5].

Because of the strong electron affinity of the fluorine molecules in the gas mixture and its detrimental effects on the discharge stability, the optimum experimental configuration for the lasers is found to be critical. In the present study we use the optical output energy as an indicator of the discharge quality to determine its sensitivity to variations in the discharge conditions such as the preionisation delay timing. In this paper we discuss the output energy of the laser as a function of the preionisation delay time, when different excitation circuits are used.

1 Experimental setup

The laser head consists of a rectangular stainless steel vessel, fitted at opposite sides with uncoated MgF_2 windows. The laser cathode is of the uniform-field type [6], the grounded anode is flat (see Fig. 1). Both electrodes are made of nickel-plated aluminium. The discharge volume is approximately $60 \times 1.5 \times 1.2$ cm ($l \times w \times h$).

Throughout the experiments the resonator mirrors are placed outside the laser vessel, to avoid contact with the fluorine-containing gas mixture. With the ArF laser a full reflecting mirror with a 10-m concave radius and a plane 70% reflection outcoupler are used. The KrF laser resonator consists of a plane full reflector and a plane 47% reflection outcoupler. The MgF_2 windows are aligned with the mirrors, to minimise reflection losses. The gas mixture of the ArF laser is 6 mbar F_2, 100 mbar Ar, 200 mbar Ne, and 3.7 bar He. For the KrF laser the same gas mixture is used, with the argon replaced by the same amount of krypton.

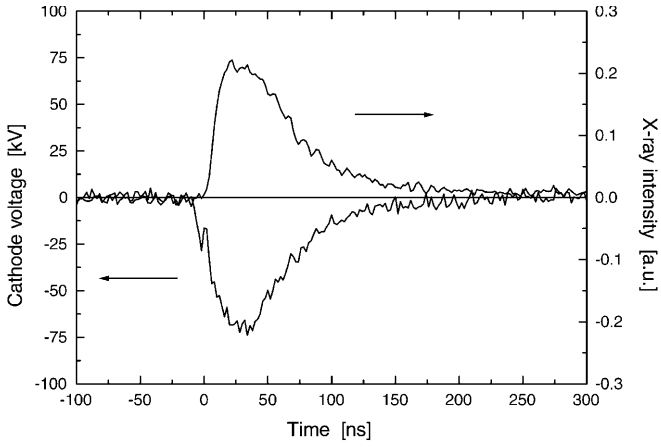

Fig. 2. Typical waveforms of the X-ray source. *Upper trace*: X-ray intensity. *Lower trace*: X-ray source cathode voltage

The preionisation of the laser gas mixture is performed by a short-pulse, high-intensity X-ray pulse. The X-ray source uses a corona-plasma cathode, charged to approximately 70 kV [7, 8]. The anode consists of a 20-μm tungsten coating on the 1-mm-thick pressure window between the X-ray source and the laser vessel. The X-rays enter the discharge volume through the pressure window and through the laser anode, which is also milled down to 1 mm to minimise the attenuation of the radiation (see Fig. 1). The X-ray source is operated using a fast, coaxial 6-stage mini-marx generator, yielding a voltage pulse length of 50 ns (FWHM) with a rise time of approximately 15 ns. Figure 2 shows the X-ray cathode voltage pulse and the resulting X-ray intensity at the centre of the discharge volume, measured using an NE102A plastic scintillator and a photomultiplier tube [8]. The X-ray pulse is capable of generating an electron density of up to 3×10^9 cm^{-3} bar^{-1} in a gas mixture equal to the ArF laser gas mixture but without fluorine. The preionisation electron density in the KrF laser gas mixture is assumed to be of the same order of magnitude [9].

2 Excitation circuits

To minimise the growth of instabilities during the pre-breakdown phase, the homogeneous preionisation electron density ($\sim 10^9$ el. cm^{-3}) should be enhanced to the discharge electron density ($\sim 10^{14}$ el. cm^{-3}) [10, 11] before inhomogeneities can arise. Net electron multiplication takes place when the interelectrode voltage V_{AC} is higher than the steady-state voltage V_{SS}. The steady-state voltage is approximately 5 kV in our setup. At voltages lower than V_{SS} there is a net electron loss, mainly by the fast attachment to fluorine [10, 12]. At $V_{AC} = V_{SS}$ the two processes are in (macroscopic) equilibrium.

To excite the laser gas mixture we use four different spiker-sustainer circuits, each designed to generate a high breakdown voltage to ensure a good electron multiplication, as well as to match the discharge impedance at V_{SS}. The circuits are all operated according to the same principle; a pulse-forming network (PFN), with a capacitance $C_{PFN} = 324$ nF, is separated by a low-inductance switch from the laser head and the peaking capacitors C_P, see Fig. 3. Once the PFN has been pulse charged, the switch is closed. A current then flows from the PFN to the much smaller peaking capacitors, $C_P = 2.8$ nF, thus generating a very fast, high voltage overshoot to start the discharge. The discharge is subsequently sustained by the current from the PFN. In order to obtain voltage matching C_{PFN} should be charged to $2V_{SS}$ [13–15].

The studied circuits differ with respect to the main switch and its operation. The switch is either a saturable inductor made of high-frequency ferrite or a triggerable multi-spark railgap. The railgap is pressurised with nitrogen, which is flowed continuously. The prepulse is generated by a mini-marx generator, equal to the X-ray source driver. The PFN is pulse charged in a few μs from a separate circuit.

In Fig. 3 the circuits with the theoretically predicted electrode voltage pulses are shown.

In the 'church' mode, Fig. 3a, the railgap is operated by means of a high voltage pulse on the trigger electrode.

In the 'swing' mode, Fig. 3b, the railgap is switched by a short prepulse on the peaking capacitors. The prepulse voltage has an opposite polarity to the main pulse, thus the voltage across the railgap increases rapidly until it breaks down [13]. By adjusting the gas pressure in the railgap its breakdown voltage is kept lower than the breakdown voltage of the laser, but higher than V_{SS}.

The 'resonant overshoot' mode, Fig. 3c, operates like the swing mode. The resonant overshoot mode is generally realised using a saturable inductor, L_{SAT}, which is switched from a high inductive state to a low inductive state by the prepulse [2, 15]. An equivalent circuit is obtained when the railgap is bridged with an inductor, L_{RG}, see Fig. 3d. The in-

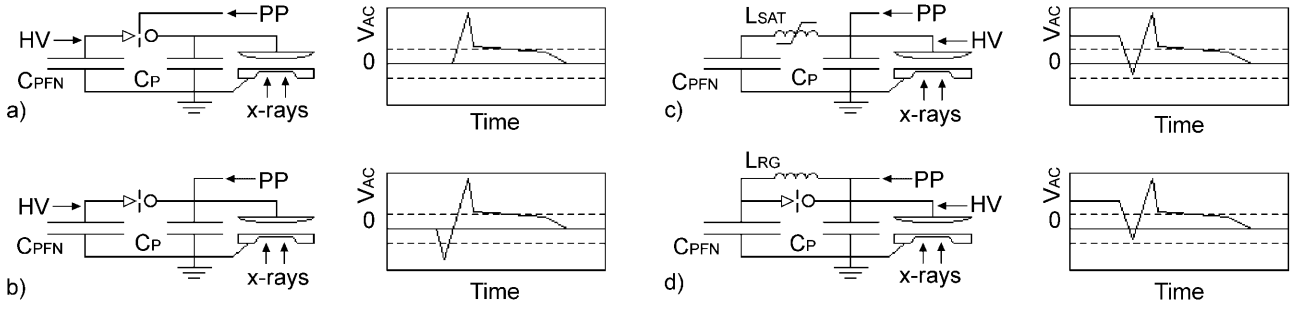

Fig. 3a–d. The studied circuits and the resulting voltage pulses. **a** 'church' mode; **b** 'swing' mode; **c** resonant-overshoot mode, saturable inductor-switched; **d** resonant-overshoot mode, railgap-switched. C_{PFN}: pulse-forming network; C_P: peaking capacitor; HV: PFN charging voltage; PP: prepulse voltage; L_{SAT}: saturable inductor; L_{RG}: inductor bridging the railgap; V_{AC}: electrode voltage. $+V_{SS}$ and $-V_{SS}$ are indicated by the *broken lines*

ductance of L_{RG} is chosen to allow the slow pulse charging of C_{PFN} while keeping the fast prepulse from vanishing into the PFN. In the resonant overshoot mode the prepulse does not get below $-V_{SS}$ in our setup.

The two resonant overshoot circuits proved to be equivalent in the operation of the laser. Therefore, we concentrated on the railgap-switched circuits, enabling a good comparison between the different circuits under otherwise unaltered circumstances.

3 Results and discussion

With each circuit a series of laser pulses is fired with different preionisation delay times $\Delta t_X = t_X - t_0$, where t_X is the start of the X-ray pulse and t_0 indicates the breakdown of the laser, see Fig. 4. To obtain a higher pumping power, the discharges are operated at higher PFN voltages than required for operation under matched conditions. The output energy E_{OUT} of each laser pulse is measured with a GenTec pyroelectric energy meter. The optical pulse is monitored with a UV-sensitive photodiode (FND100Q) through the rear laser mirror and a 193-nm or a 248-nm filter. In Fig. 5 the output energy as a function of Δt_X for the church mode, the swing mode and the railgap-switched resonant-overshoot mode are shown for the ArF laser. In Fig. 6 the results for the KrF laser are shown.

The church mode and the resonant-overshoot mode both exhibit a very short delay time window in which output can be generated, with the resonant overshoot mode yielding slightly more output than the church mode. With the swing mode longer preionisation delay times can be allowed. The output then shows a clear maximum and a local minimum of near-zero energy. With short delay times, Δt_X shorter than ~ 22 ns, all three excitation modes show the same behaviour. The results are equal for both lasers.

The output of the KrF laser is higher than that of the ArF laser and the preionisation delay windows for the different modes are slightly longer with KrF than with ArF. This is likely to be caused by the KrF laser having a higher gain. Similarly, when the pumping power of the ArF laser is decreased, by lowering the PFN voltage, the output energy per pulse drops and the preionisation window gets smaller, see Fig. 7.

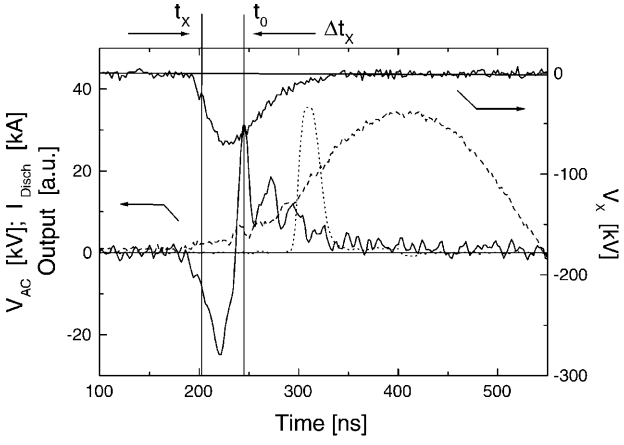

Fig. 4. Typical waveforms of a swing-mode pulse with ArF and the definition of the preionisation delay time Δt_X. *Left axis*: —: electrode voltage V_{AC}, −−: discharge current I_{Disch}, ···: optical pulse (24 ns FWHM, 34 mJ). *Right axis*: —: X-ray source cathode voltage V_X. Charging voltages: $V_{PFN} = 22$ kV, $V_{PP} = 20$ kV. $\Delta t_X = -44$ ns

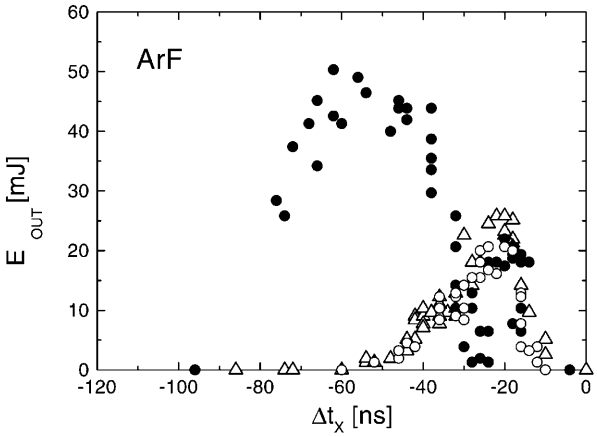

Fig. 5. ArF laser output energy E_{OUT} as a function of the preionisation delay time Δt_X with different excitation circuits. ○: church mode, ●: swing mode, △: resonant-overshoot mode (railgap). Charging voltages: $V_{PFN} = 27$ kV, $V_{PP} = 20$ kV

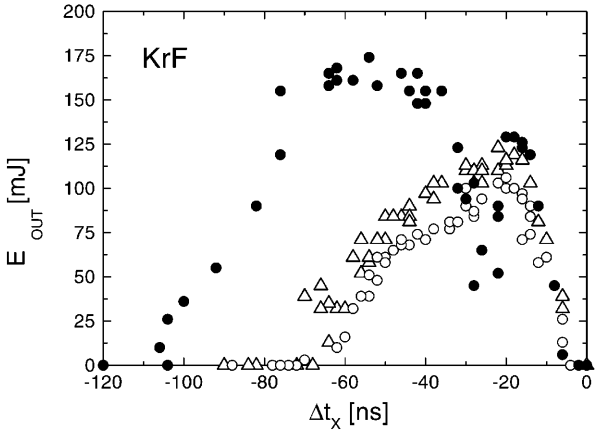

Fig. 6. KrF laser output energy E_{OUT} as a function of the preionisation delay time Δt_X with different excitation circuits. ○: church mode, ●: swing mode, △: resonant-overshoot mode (railgap). Charging voltages: $V_{PFN} = 27$ kV, $V_{PP} = 20$ kV

We can explain our results when the processes leading to the breakdown of the laser gas mixture are taken into account, and the fact that a F_2-containing discharge inherently gets unstable. Discharge instabilities are developed in a few ns from minor preionisation inhomogeneities, electrode irregularities, cathode hotspots, and/or local gas density fluctuations [10, 16–18]. Unstable discharges generate low or no laser output because pumping power is lost in the discharge streamers and because plasma filamentation disturbs the optical properties of the medium.

The fast growth of discharge instabilities is reflected in our results. In the church mode and in the resonant-overshoot mode output energy is obtained only when the X-ray pulse overlaps the voltage pulse at $V_{AC} > V_{SS}$, prior to the breakdown, see Figs. 3 and 4. When the X-ray pulse starts too close to the discharge breakdown, there is insufficient time for the multiplication process to generate a homogeneous electron density that is high enough for a homogeneous breakdown [2, 19]. When the X-ray pulse is applied too early, i.e.

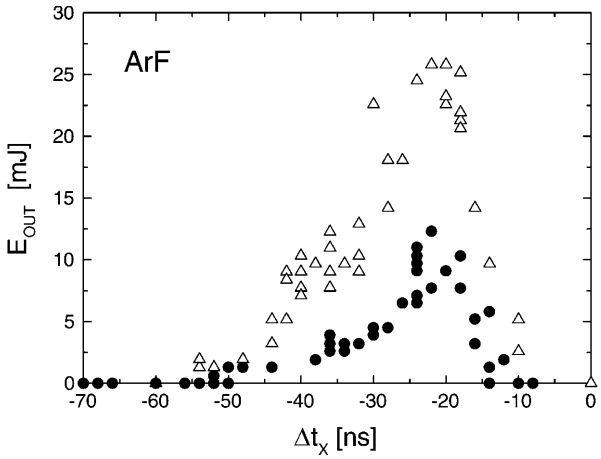

Fig. 7. ArF laser output energy E_{OUT} as a function of the preionisation delay time Δt_{X} and of the PFN voltage V_{PFN}. Resonant overshoot mode (railgap). Charging voltages: △: $V_{\mathrm{PFN}} = 27\,\mathrm{kV}$, ●: $V_{\mathrm{PFN}} = 23\,\mathrm{kV}$, $V_{\mathrm{PP}} = 20\,\mathrm{kV}$

before $V_{\mathrm{AC}} > V_{\mathrm{SS}}$, preionisation electrons will be lost due to the rapid attachment to F_2. Furthermore, the negative voltage on the cathode will push the present electrons away from it, leaving a depleted layer [19, 20]. These processes lead to inhomogeneous electron densities during the discharge formation. Thus poor discharges with low output energies result.

Preionisation of the gas mixture can also be performed by detaching electrons from F^-, as proposed by Hsia [21]. This process is approximately 0.03% efficient, thus an initial electron density of $n_{\mathrm{e0}} \approx 3 \times 10^{10}\,\mathrm{cm}^{-3}$ is required during a long time [9, 20]. In our setup this preionisation level cannot be reached. Furthermore, we observe no lasing at long preionisation delays, which is the regime of the process. Therefore, we assume the effective preionisation to be due to the directly generated electron density only.

In the swing mode the two time windows in which output is generated are probably caused by the electrode voltage being higher than V_{SS} both during the prepulse and during the overshoot, see Figs. 3b and 4. The minimum in the output energy corresponds to the application of the maximum of the X-ray pulse during the voltage cross-over from $-V_{\mathrm{SS}}$ to $+V_{\mathrm{SS}}$ inbetween the prepulse and the overshoot.

In the resonant-overshoot mode the electrodes are initially charged to the PFN voltage, which is well above V_{SS}. However, the voltage drops below V_{SS} for approximately 25 ns when the prepulse is applied, see Figs. 3c and d. During this time the possible beneficial effects of the initial presence of a high voltage are cancelled. Preionising during the PFN charging leads to a spontaneous breakdown some time before the application of the prepulse, in which case there is no output generated.

The risetime of the voltage on the peaking capacitors is equal in all circuits, because it is determined by the self-inductance of the circuit between the PFN and the peaking capacitors. This explains the similarity in the performance of all three excitation modes at low Δt_{X}.

The higher output energy when using the swing mode with longer preionisation delay times is probably caused by the following effect: during the prepulse the electron multiplication due to $V_{\mathrm{AC}} > V_{\mathrm{SS}}$ is very efficient because the electron attachment to fluorine is reduced at high E/N values. Since the laser does not break down during the prepulse, it acts as an extra long preionisation multiplication time.

In order to produce an initially uniform discharge it is necessary for individual avalanches to grow and overlap, perpendicular to the field, prior to them reaching a given size [19]. During the prepulse the heads of the individual electron streamers grow radially while the tail extends towards the cathode. At the voltage reversal, before the actual breakdown, both the electrons in the head and those in the tail will reverse in direction. If the streamer heads have grown to the critical size at that time, this results in a more widely spread charge distribution at the breakdown than simple unipolar streamers would. Thus it gives a better streamer overlap and hence a better laser performance. If, on the other hand, the streamer heads have not yet grown enough at the moment of the voltage reversal, the reversing electrons of the avalanche head will sense the lingering positive space-charge field of the streamer tail. This will decrease the further lateral growth of the avalanche heads, resulting in a very inhomogeneous charge distribution at the moment of breakdown. The resulting poor discharges are likely to cause the low output of the swing mode at $\Delta t_{\mathrm{X}} \approx 22$ ns. These effects may be increased by the increased electron attachment to F_2 at low electric fields.

Another reason for a higher output energy when using the swing mode with longer Δt_{X} is probably that although during the prepulse a depleted cathode layer is formed, during the following voltage overshoot of the opposite polarity the present electrons are accelerated in the reverse direction, refilling the depleted area [22]. Therefore the subsequent breakdown starts from a much more homogeneous electron density. The result is a better discharge quality and a higher output energy.

With an increasing preionisation delay the electron density at the start of the overshoot increases in the swing mode, due to the multiplication during the prepulse. A higher electron density at the start of the overshoot is translated into a lower breakdown voltage, see Fig. 8. From Fig. 8 it can be seen that the breakdown voltage of the KrF laser rises quickly at delays Δt_{X} longer than 100 ns, i.e. when the X-ray pulse is applied before $V_{\mathrm{AC}} > V_{\mathrm{SS}}$. This can again be re-

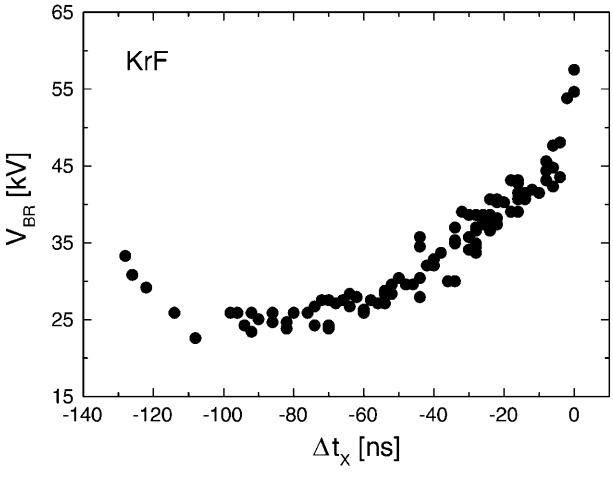

Fig. 8. The breakdown voltage V_{BR} of the KrF laser gas mixture as a function of the preionisation delay time Δt_{X}. Swing mode. Charging voltages: $V_{\mathrm{PFN}} = 27\,\mathrm{kV}$, $V_{\mathrm{PP}} = 20\,\mathrm{kV}$

lated to the electron attachment of the fluorine, causing fewer free electrons to be present when V_{AC} increases over V_{SS}. At these long preionisation delays the laser generates no output, caused by minor inhomogeneities growing into filaments during the pre-breakdown phase. This process of plasma filamentation during the pre-breakdown phase already affects the optical performance from $\Delta t_X \gtrsim 60$ ns.

4 Conclusion

We have shown that the timing of the application of the X-ray preionisation of a discharge-excited ArF and KrF laser has a profound influence on the performance of the laser. The effect is clear for three different spiker-sustainer excitation pulses.

The optimum output energy in both lasers was obtained in the so-called swing mode, which uses a high prepulse of opposite polarity to the main pulse to increase the preionisation electron density in the laser gas, prior to the breakdown, for obtaining a better discharge quality. The preionisation timing is best when the leading edge of the X-ray pulse coincides with the prepulse voltage increasing over V_{SS}.

Acknowledgements. The authors wish to thank H.M.J. Bastiaens for many stimulating discussions. The present work has been supported by the Netherlands Technology Foundation STW.

References

1. F.A. van Goor, W.J. Witteman, J.C.M. Timmermans, J. van Spijker, J. Couperus: Proc. SPIE **2206**, 30 (1994)
2. R.S. Taylor, K.E. Leopold: Appl. Phys. B **59**, 479 (1994)
3. M. Ohwa, M. Obara: J. Appl. Phys. **63**, 1306 (1988)
4. A.A. Zhupikov, A.M. Razhev: Quantum Electron. **27**, 665 (1997)
5. A.A. Zhupikov, A.M. Razhev: Quantum Electron. **28**, 667 (1998)
6. G.J. Ernst: Opt. Commun. **49**, 275 (1984)
7. S.J. Scott: Appl. Phys. B **56**, 201 (1993)
8. F.A. van Goor: J. Phys. D: Appl. Phys. **26**, 404 (1993)
9. M. Steyer, H. Voges: Appl. Phys. B **42**, 155 (1987)
10. M.R. Osborne: Appl. Phys. B **45**, 285 (1988)
11. S. Nagai, H. Furuhashi, A. Kono, Y. Uchida, T. Goto: IEEE J. Quantum Electron. **QE-34**, 942 (1998)
12. P.J. Chantry: In *Applied Atomic Collision Physics*, ed. by E.W. McDaniel, W.L. Nighan, Vol. 3 (Academic Press, New York, NY 1982) p. 35
13. W.H. Long, M.J. Plummer, E.A. Stappaerts: Appl. Phys. Lett. **43**, 735 (1983)
14. M.R. Osborne, P.W. Smith, M.R. Hutchinson: Opt. Commun. **52**, 415 (1985)
15. J.W. Gerritsen, A.L. Keet, G.J. Ernst, W.J. Witteman: J. Appl. Phys. **67**, 3517 (1990)
16. M.J. Kushner: IEEE Trans. Plasma Sci. **19**, 387 (1991)
17. R. Dreiskemper, W. Bötticher: IEEE Trans. Plasma Sci. **23**, 987 (1995)
18. J. Coutts, C.E. Webb: J. Appl. Phys. **59**, 704 (1986)
19. J.I. Levatter, S.C. Lin: J. Appl. Phys. **51**, 210 (1980)
20. R.S. Taylor: Appl. Phys. B **41**, 1 (1986)
21. J. Hsia: Appl. Phys. Lett. **30**, 101 (1977)
22. F.A. van Goor, J.C.M. Timmermans, W.J. Witteman: Opt. Commun. **124**, 56 (1996)